Proceedings of the ASME 2013 Conference on Smart Materials, Adaptive Structures and Intelligent Systems
SMASIS2013
September 16-18, 2013, Snowbird, Utah, USA

SMASIS2013-3258

MODELING AND CONTROL OF LOZENGE-SHAPED DIELECTRIC ELASTOMER GENERATORS

Giacomo Moretti **Marco Fontana** **Rocco Vertechy**

PERCRO SEES, TeCIP Institute, Scuola Superiore Sant'Anna
Piazza Martiri della Libertà 33, Pisa, 5612, Italy
E-mail: m.fontana@sssup.it, r.vertechy@sssup.it

ABSTRACT

Dielectric Elastomers (DEs) are a very promising technology for the development of energy harvesting devices based on the variable-capacitance electrostatic generator principle. As compared to other technologies, DE Generators (DEGs) are solid-state energy conversion systems which potentially feature: 1) large energy densities, 2) good energy conversion efficiency that is rather independent of cycle frequency, 3) easiness of manufacturing and assembling, 4) high shock resistance, 5) silent operation, 6) low cost. Envisioned applications for DEGs are in devices that convert ocean wave energy into usable electricity.

This paper introduces the Lozenge-Shaped DEG (LS-DEG) that is a specific type of planar DE transducer with one degree of freedom. A LS-DEG consists of a planar DE membrane that is connected along its perimeter to the links of a parallelogram four-bar mechanism. As the mechanism is put into reciprocal motion, the DE membrane varies its capacitance that is then employed as a charge pump to convert external mechanical work into usable electricity.

Specifically, this paper describes the functioning principle of LS-DEGs, and provides a comparison between different hyper-elastic models that can be used to predict the energy harvesting performances of realistic prototypes. Case studies are presented which address the constrained optimization of LS-DEGs subjected to failure criteria and practical design constraints.

INTRODUCTION

Dielectric Elastomers (DEs) are deformable dielectrics, which can experience finite deformations when subjected to large electric fields and which alter the existing electrostatic fields in response to the undergone deformations.

DEs have been largely studied for actuation and sensing applications. However, in the last decade several researches have demonstrated that they can be successfully employed as electricity generators [1]. DE Generators (DEGs) working principle is based on a capacitor whose dielectric layer is deformed, resulting in large variations of its capacitance. Such a variable capacitor works as a charge pump and makes it possible to convert the mechanical energy introduced for the deformations into usable electrical energy.

One of the most promising fields of application for DEGs is in the wave energy sector. Present technologies for Wave Energy Converters (WECs) are based on traditional hydraulic and mechanical components made of bulky, heavy, costly and corrosion-sensitive materials. The development of WECs could be largely simplified through the use of DEGs, thanks to their: 1) large energy densities, 2) good energy conversion efficiency that is rather independent of cycle frequency, 3) easiness of manufacturing and assembling, 4) high shock resistance, 5) silent operation, 6) low cost. Preliminary investigations on the use of DEGs for the implementation of WECs can be found in [2-5].

The general working principle of DEGs and the maximum energy per unit volume that they can convert have been investigated by Koh et al. [6], who proposed a procedure for the determination of theoretical limits based on electromechanical rupture and instability criteria. Pelrine et al. [1] have measured energy densities up to 0.4 J/g and have estimated maximum theoretical energy densities up to 1.5 J/g. Jean-Mistral et al. [7] and Koh et al. [8] investigated a configuration of planar DEG in a uniform equi-biaxial state of deformation, assessing a maximum converted energy of 3.2 J/g and 1.7 J/g respectively. Specific DEG designs with conical [9-11] or spherical shape [12] have also been investigated.

In the present work, the Lozenge-Shaped DEG (LS-DEG) is studied via preliminary experiments and theoretical arguments. In particular, the paper: 1) presents three hyper-elastic models of the LS-DEG that are fitted to a set of experimental tests conducted on a commercial DE membrane; 2) introduces a model to predict the failure conditions that limit the maximum electrical energy per unit volume that can be converted by LS-DEGs; 3) defines a procedure for the choice of the optimal design parameters that maximize the electricity

generation performances of LS-DEGs; 4) analyzes the influence of the chosen hyper-elastic model in the selection of such optimal design parameters.

The operation of the lozenge-shaped DE transducer has been examined by Vertechy et al. in [13], who proposed a mathematical procedure that optimizes the behavior of the device when used as an actuator. However, the analysis and optimization of the LS-DEG requires a different approach and has not been presented in previous researches.

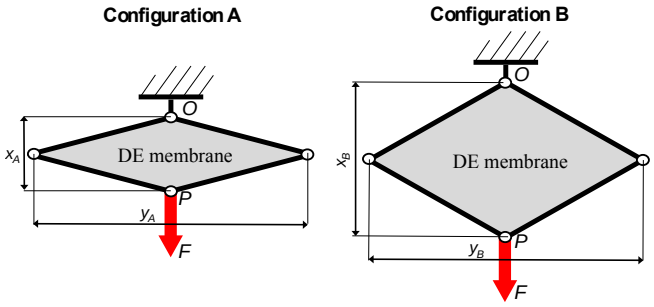

Figure 1 – Scheme of the Lozenge-Shaped DE Generator (LS-DEG). Configuration A on the left and Configuration B on the right.

THE LOZENGE SHAPED DE GENERATOR

The LS-DEG consists in a planar incompressible DE membrane that is pre-stretched and clamped to a rigid frame shaped as four-bar mechanism with equal-length links (see Figure 1). The LS-DEG position can be uniquely defined by the variable x (hereafter also called 'transducer length' or 'longitudinal length'), with which we indicate the distance between the centers O and P of the two opposite joints of the four-bar mechanism (see Figure 1); while the distance between the other two opposite centers of the revolute pairs is hereafter indicated with the variable y and is also called 'transversal length'.

With the variation of x, the DE membrane deforms uniformly and the deformation is uniquely identified by the first and second principal stretches, λ_1 (along the x direction) and λ_2 (along the y direction). The DE membrane has compliant electrodes on both sides, forming a deformable parallel-plate capacitor whose capacitance is a function of x. We consider the loading case in which an external force is applied along the x direction at the joint P and the opposite vertex O is connected through a revolute joint to the ground.

The working principle of the LS-DEG can be briefly described as follows. Let's consider the reciprocating motion of the LS-DEG while it is opening and closing under the action of an external force, and correspondingly the length x is varying from a value $x = x_A$ to $x = x_B$ (with $x_B > x_A$).

When the transducer length is changed from x_A to x_B (loading phase), elastic energy is stored in the DE membrane. In the position $x = x_B$, the DE membrane is provided with an amount of charge and is electrically activated. During the reverse movement, from the position x_B up to x_A (unloading phase), the force exerted by the DE membrane to the four-bar mechanism is lower due to the electric load. The difference between the mechanical work performed during the loading and unloading phases represents the amount of electric energy generated by the LS-DEG.

From the functional point of view, the LS-DEG can be seen as a linear transducer which produces electric energy from the reciprocating motion imposed by an external oscillating force. These generators may be successfully employed as Power Take Off (PTO) systems for a number of WEC devices, like buoys or flaps that currently make use of traditional hydraulics or electromagnetic generators.

MECHANICAL CHARACTERIZATION AND MODELING

This section describes the materials and methods employed to experimentally characterize the force-displacement response of a LS-DEG. Three analytical hyper-elastic models are considered and fitted to the same experimental data.

Experimental Setup

The DE employed in the present work, is the acrylic elastomer VHB-4905 by 3M that is available in thin films with 0.5 mm thickness.

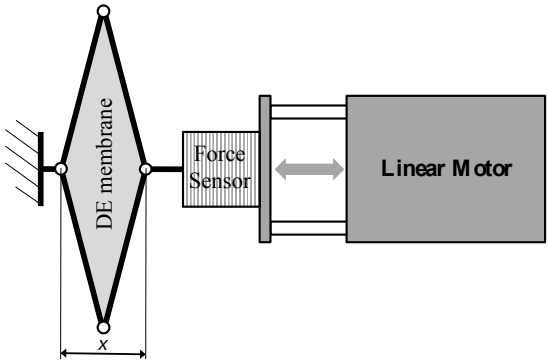

Figure 2 - Test rig equipped with linear servomotor and force sensor.

In order to produce experimental results that are suited to the considered application, mechanical tests have been performed on a test rig (see Figure 2) which comprises:

- a lozenge mechanism with side lengths ℓ=80 mm, whose links have been designed to easily allow the connection of a DE membrane along its perimeter;
- a set of membranes made of three layers of 0.5 mm thick films for a total thickness of 1.5 mm (when unstretched);
- a brushless linear motor (P01-37x120F-HP by LinMot™) with a high resolution linear encoder that is employed to impose the reciprocating force/motion to the LS-DEG;
- driving and control electronics in order to regulate the LS-DEG motion according to the desired position profiles;
- a single axis load cell and a 13 bits acquisition electronics employed to measure the force of the LS-DEG along the x direction.

Such setup guarantees a force accuracy and resolution better than 25 mN, a position accuracy and resolution better than 0.05 mm and a maximum acquisition rate of 2kHz.

Characterization Methods

Different experiments have been conducted by varying the longitudinal length x of the lozenge membrane and measuring the corresponding value of the longitudinal force F. Each sample of material has been subjected to several loading-unloading cycles programming a saw-tooth position profile oscillating from x_A =20 mm to x_B =85 mm.

Since this study focuses on the quasi static behavior of LS-DEGs, experiments have been conducted at the low speed of 0.5 mm/s. This reduces visco-elastic effects and makes it possible to acquire the desired equilibrium response curves. Acquisition rate has been set to 20Hz. Five different samples of DE membrane (M1-M5) with different pre-stretches λ_{1p} (longitudinal direction) and λ_{2p} (transversal direction) have been tested in order to gather the required data for determining constitutive parameters of the employed DE material [14].

ID	λ_{1p}	λ_{2p}	$\boldsymbol{\lambda_1}$ (min-max)	$\boldsymbol{\lambda_2}$ (min-max)
M1	12.56	3.90	2.22 – 9.44	4.67 – 5.47
M2	11.31	3.90	2.00 – 8.50	4.67 – 5.47
M3	9.42	3.90	1.67 – 7.08	4.67 – 5.47
M4	9.42	3.24	1.67 – 7.08	3.88 – 4.55
M5	11.31	4.71	2.00 – 8.50	5.64 – 6.61

Table 1: Data of pre-stretches (at $x_p = \ell\sqrt{2}$), range of longitudinal displacement and limit stretches for the 5 DE membrane samples (M1-M5).

Pre-stretches λ_{1p} and λ_{2p} can be given at any arbitrary reference position x_p. In the present work, pre-stretches are referred to the configuration at which the links of the lozenge form right angles, i.e. $x_p=\ell\sqrt{2}$. It is worth to notice that such a configuration is not necessarily reached during the operation of the device, but it is always possible to mathematically refer the pre-stretches to that configuration. Ten loading-unloading cycles have been acquired for each measurement (Table 1).

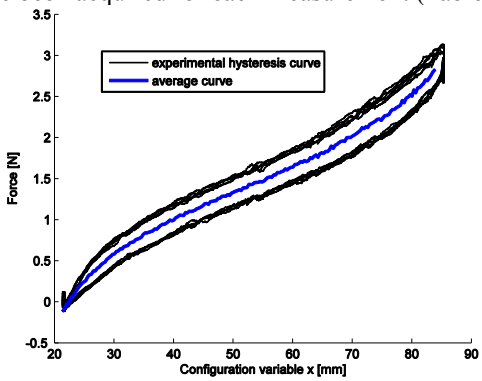

Figure 3 – Cyclic test of membrane 3 (M3): plot of the measured force-displacement curves.

The data have been averaged on the last seven of the ten cycles since the response of the material becomes repeatable after the first three cycles. Experimental data have been acquired for loading-unloading curves and filtered (using moving average filter with span of 41 samples). An example of the resulting loading-unloading cycle is represented in Figure 3. As reported, the cyclic response shows some remaining hysteresis. The equilibrium response curve is obtained as the average between the loading and unloading curves (see Figure 3).

Hyperelastic Models and Fitting of Results

The hyper-elastic behavior of the acrylic material VHB-4905 can be described through the strain-energy function ψ [15]. The material is assumed incompressible, thus the stretch in the z direction (along the normal to the lozenge surface) can be express by

$$\lambda_3 = \left(\lambda_1\lambda_2\right)^{-1}. \tag{1}$$

Based on the lozenge geometry, the stretches in the x-y plane can be written as functions of the pre-stretches and of the variable x as

$$\lambda_1 = \lambda_{1p}\, x/x_p\,, \tag{2}$$

$$\lambda_2 = \lambda_{2p}\, y/y_p = \lambda_{2p}\sqrt{\left(4\ell^2 - x^2\right)/\left(4\ell^2 - x_p^{\,2}\right)}\,. \tag{3}$$

In absence of electrical activation, if the material is free to expand in z direction, the principal stresses are given by equations (4):

$$\sigma_1 = \lambda_1\frac{\partial\psi(\lambda_1,\lambda_2)}{\partial\lambda_1}\,,\quad \sigma_2 = \lambda_2\frac{\partial\psi(\lambda_1,\lambda_2)}{\partial\lambda_2}\,. \tag{4}$$

In static condition and in absence of electrical activation, the elastic force F_{off} is given by [13]

$$F_{off}(x) = \frac{t_0}{2}\left(\frac{\sqrt{4\ell^2 - x_p^2}}{\lambda_{2p}}\frac{\partial\psi}{\partial\lambda_1} - \frac{x\,x_p}{\lambda_{1p}\sqrt{4\ell^2 - x^2}}\frac{\partial\psi}{\partial\lambda_2}\right). \tag{5}$$

Equation (5) provides an analytic relation between force F_{off} versus the position x through the derivatives of the strain-energy function. Equation (5) has been used to fit experimental data through the Levenberg-Marquardt algorithm [16], implemented in the Matlab Optimization Toolbox.

By introducing the first deformation invariant [15]

$$I_1(\lambda_1,\lambda_2) = \lambda_1^2 + \lambda_2^2 + \lambda_3^2 = \lambda_1^2 + \lambda_2^2 + \lambda_1^{-2}\lambda_2^{-2}\,, \tag{6}$$

the experimental results of the 5 DE membranes considered in Table 1 have been fitted to three different hyperelastic models: Ogden, Yeoh and Gent [17]. The stability of the models has been verified in the working range of interest for this particular application. For each model, Table 2 resumes the constitutive parameters resulting from the experimental fitting. Comparison between fitted models and experimental results is provided in Figure 4. For picture clearness, only the results for 3 DE membrane samples are shown, with markers representing experimental curves.

FAILURE CONDITIONS

In this section, the failure conditions that limit the maximal energy density (per unit volume of the employed DE material) that can be converted by LS-DEGs are presented in analytical form.

Model	Strain-energy function form	Experimental parameters
Ogden (2^{nd} ord.)	$\psi = \sum_{i=1}^{2} \frac{\mu_i}{\alpha_i}\left(\lambda_1^{\alpha_i} + \lambda_2^{\alpha_i} + \lambda_3^{\alpha_i} - 3\right) = \sum_{i=1}^{2} \frac{\mu_i}{\alpha_i}\left(\lambda_1^{\alpha_i} + \lambda_2^{\alpha_i} + \lambda_1^{-\alpha_i}\lambda_2^{-\alpha_i} - 3\right)$	$[\mu_1 \ \mu_2]$=[-1.01 8e3] Pa $[\alpha_1 \ \alpha_2]$=[-2.0 2.48]
Yeoh	$\psi = C_1\left(I_1 - 3\right) + C_2\left(I_1 - 3\right)^2 + C_3\left(I_1 - 3\right)^3$	C_1 = 6.26e3 Pa C_2 = 22.6 Pa C_3 = 3.13e-2 Pa
Gent	$\psi = -a \ln\left(\frac{I_m - I_1}{I_m - 3}\right)$	a = 4.09e6 Pa I_m = 430.9

Table 2: Models that have been considered for the fitting of experimental data and relative parameters obtained via Levenberg-Marquardt algorithm [16].

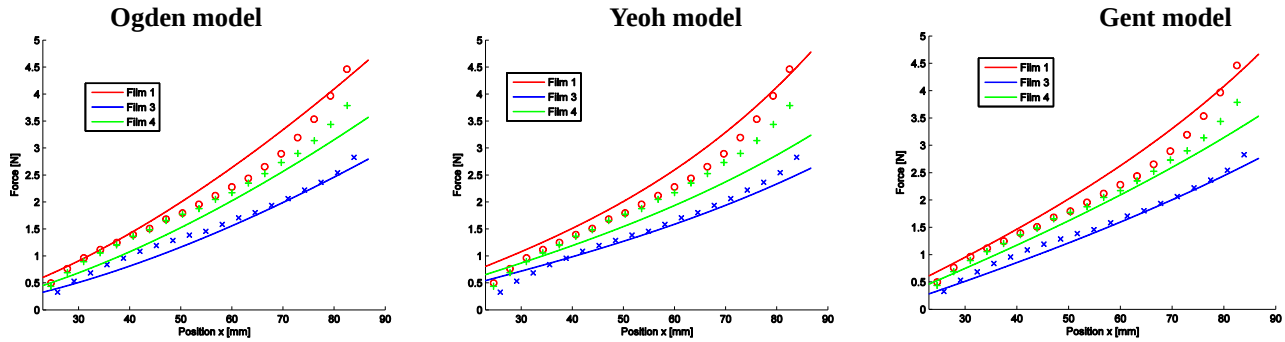

Figure 4 - Fitting of the experimental data plotted for 3 of the 5 tested membranes. Markers show experimental data while continuous lines show model predictions

According to previous studies [8], the maximum energy density that can be produced by a DEG is limited by different failure mechanisms of the employed DE membrane: 1) electrical breakdown, 2) loss of tension, and 3) mechanical rupture. These failure conditions can be represented as limit curves on the *Q*-*V* plane, where *Q* and *V* are the charge and the electric potential difference that are applied between the electrodes of the considered DEG [8]. Since the electrical work can be expressed as the integral of the voltage over the charge, the area enclosed by such limit curves in the *Q*-*V* plane represents the maximal energy that can be converted by a specific DEG.

Let x and y represent the dimensions of the LS-DEG diagonals in a generic deformed configuration, and let t and t_0 be the thicknesses of the membrane in the actual and in the undeformed configuration respectively.

By simple geometrical considerations, from equations (2) and (3) we can write λ_2 as a function of λ_1:

$$\lambda_2 = \lambda_{2p}\sqrt{\left(4\ell^2 - x_p^2\lambda_1^2 \big/ \lambda_{1p}^2\right) \big/ \left(4\ell^2 - x_p^2\right)}. \qquad (7)$$

Then, by the definition of capacitance (namely, $C=Q/V=\varepsilon xy/2t = \varepsilon x^2y^2/4B$, where ε is the dielectric constant of the considered DE material and B, $B = xyt/2$, is the volume of the considered DE membrane), λ_1 and λ_2 can be rewritten as functions of Q and V:

$$\lambda_1 = \frac{\lambda_{1p}}{x_p}\sqrt{2\ell^2 - 2\sqrt{\ell^4 - BQ/\varepsilon V}}\ , \qquad (8)$$

$$\lambda_2 = \frac{\lambda_{2p}}{y_p}\sqrt{2\ell^2 + 2\sqrt{\ell^4 - BQ/\varepsilon V}}\ . \qquad (9)$$

From these equations, it is easy to see that, on the *Q*-*V* plane, the lines representing iso-stretch transformations (that means, transformations that occur with the LS-DEG in a fixed position) are straight lines passing through the origin.

For what concerns the stress, the electrical activation of the DE membrane is responsible for a planar stress, σ_{em}, of electrostatic origin in the form $\sigma_{em}=\varepsilon E^2$ [13], with E being the electric field acting across the DE membrane. Thus, for the activated case, equations (4) become

$$\sigma_1 = \lambda_1 \frac{\partial \psi(\lambda_1, \lambda_2)}{\partial \lambda_1} - \sigma_{em}, \qquad (10)$$

$$\sigma_2 = \lambda_2 \frac{\partial \psi(\lambda_1, \lambda_2)}{\partial \lambda_2} - \sigma_{em}, \qquad (11)$$

where the hyper-elastic free-energy function ψ is given in one of the forms presented in the previous section.

Based on the preceding equations, the failure conditions of LS-DEG are next described as limit curves in the *Q*-*V* plane.

Geometric constraint: in equations (8) and (9), the argument of the square root has to be positive, which yields the limit curve

$$V = BQ/\varepsilon\ell^4 . \quad (12)$$

This physically means that the maximum allowable value for the LS-DEG capacitance occurs for $x = \sqrt{2}\ell$. Configurations given by $x \geq \sqrt{2}\ell$ are not considered, since they bring to a reduction of the capacitance.

Electric breakdown: the electric field E acting across the LS-DEG cannot exceed the dielectric strength E_{BD} of the considered DE material, namely $E \leq E_{BD}$. Since

$$E = V / t , \quad (13)$$

by the definition of capacitance, the electric breakdown condition yields the following limit curve

$$VQ = \varepsilon B E_{BD}^2 , \quad (14)$$

which describes a hyperbola in the Q-V plane.

Mechanical rupture: the mechanical rupture of DE materials is usually expressed as a limitation on the values of the stretches. For LS-DEGs, there are two rupture conditions: $\lambda_1 \leq \lambda_u$ and $\lambda_2 \leq \lambda_u$, where λ_u is the ultimate stretch before mechanical failure. Using equations (8) and (9), the rupture conditions yield the following limit curves

$$V = \frac{B}{\varepsilon} Q \cdot \left(\ell^4 - \left(\ell^2 - \frac{x_p^2 \lambda_u^2}{2\lambda_{1p}^2} \right)^2 \right)^{-1} , \quad (15)$$

$$V = \frac{B}{\varepsilon} Q \cdot \left(\ell^4 - \left(\ell^2 - \frac{y_p^2 \lambda_u^2}{2\lambda_{2p}^2} \right)^2 \right)^{-1} . \quad (16)$$

On the Q-V plane, these equations represent straight lines passing through the origin of the axes. With regard to the value of λ_u, according to [13], λ_u is assumed equal to 5.5. This is a rather conservative value that has been verified with the experimental investigations described in the previous section.

Loss of tension: to function properly, the DEG membrane should not wrinkle. This requires equations (10) and (11) to be positive. Manipulating the expression for the electrically induced stress, namely

$$\sigma_{em} = QV/B , \quad (17)$$

the loss-of-tension condition for x and y directions yields the following limit curves

$$\lambda_1 \frac{\partial \psi}{\partial \lambda_1} = QV/B , \quad \lambda_2 \frac{\partial \psi}{\partial \lambda_2} = QV/B . \quad (18)$$

Among all the failure conditions, loss of tension is the only one that depends on the constitutive equations of the material. Thus, the prediction of loss of tension is generally related to the specific form of the free-energy function that is chosen to describe the elastic behavior of the LS-DEG.

The set of limit curves defined by equations (12), (14)-(16) and (18) determines the operation domain of the LS-DEG in the Q-V plane. In order to generalize the discussion, making it fit to any possible choice of LS-DEG geometry, equations are next reduced in dimensionless form.

We introduce the following dimensionless parameters:

$$x^* = x/\ell , \quad y^* = y/\ell = \sqrt{4 - x^{*2}} , \quad (19)$$

$$Q^* = Q\left(\varepsilon E_{BD} \ell^2\right)^{-1} , \quad (20)$$

$$V^* = V\left(E_{BD} B/\ell^2\right)^{-1} . \quad (21)$$

Referring to the new variables, the limit curves assume the expressions below:

Dimensionless Geometric Constraint (GC):

$$V^* = Q^* . \quad (22)$$

Dimensionless Electric Breakdown Condition (BD):

$$Q^* V^* = 1 . \quad (23)$$

Dimensionless Mechanical Rupture Condition (RC):

$$V^* = Q^* \cdot \left(1 - \left(1 - \frac{x_p^{*2} \lambda_u^2}{2\lambda_{1p}^2} \right)^2 \right)^{-1} , \quad (24)$$

$$V^* = Q^* \cdot \left(1 - \left(1 - \frac{y_p^{*2} \lambda_u^2}{2\lambda_{2p}^2} \right)^2 \right)^{-1} . \quad (25)$$

Dimensionless Loss of Tension Condition (LoT):

$$\lambda_1 \frac{\partial \psi}{\partial \lambda_1} = \varepsilon E_{BD}^2 Q^* V^* , \quad (26)$$

$$\lambda_2 \frac{\partial \psi}{\partial \lambda_2} = \varepsilon E_{BD}^2 Q^* V^* . \quad (27)$$

These equations make it possible to compare LS-DEGs having different geometric dimensions and that employ the same DE material.

ENERGY CONVERSION CYCLE OPTIMIZATION

The limits determined by the introduced electromechanical failure conditions identify the usable working space (namely, the area A_c in the Q^*-V^* plane) where the LS-DEG can operate safely. Evaluation of the practical energy, En, that can be generated requires the definition of a suitable Energy Conversion Cycle (ECC); namely, the cyclical sequence of electromechanical transformations that is commanded to the LS-DEG in order to convert mechanical energy into electricity.

In the Q^*-V^* plane, any possible ECC describes a closed surface, whose area represents the generated energy in dimensionless form; namely

$$En^* = En\left(\varepsilon E_{BD}^2 B\right)^{-1} . \quad (28)$$

Here, an ideal ECC is considered which perfectly follows the limit curves defined by equations (22)-(27). This provides the maximal energy density for the LS-DEG (that is, $En^*=A_c$).

For a given DE, dimensionless GC, BD and RC curves are univocally determined. Therefore, the size of the area A_c only depends on LoT curves, which are functions of membrane pre-stretches λ_{1p} and λ_{2p}. In addition, the specific shape of LoT curves also depends on the particular form chosen for the hyper-elastic free-energy function of the considered DE material. This is shown in Figure 5, which reports (in the Q^*-V^* plane) the ECCs of LS-DEGs that hold for the three different hyper-elastic models considered in Table 2 (and for the same E_{BD} = 50 MV/m, λ_{1p} = 6 and λ_{2p} = 2). Specifically, the three plots highlight that different hyperelastic models predict different values of producible electrical energy.

In the following sections, ECCs for LS-DEGs are optimized for the three hyper-elastic models considered in Table 2. The analysis is conducted by considering a first case of constant dielectric strength, and a second case in which the dielectric strength depends on the stretch state.

Constant Electric Breakdown Condition

For the constant dielectric strength case, two different limit values have been considered: E_{BD} = 50 MV/m and E_{BD} = 70 MV/m. The plots in Figure 6 represent the producible energy (per unit volume of employed DE material) as a function of λ_{1p}, for different values of λ_{2p}, for each hyper-elastic model and for each chosen value of E_{BD}.

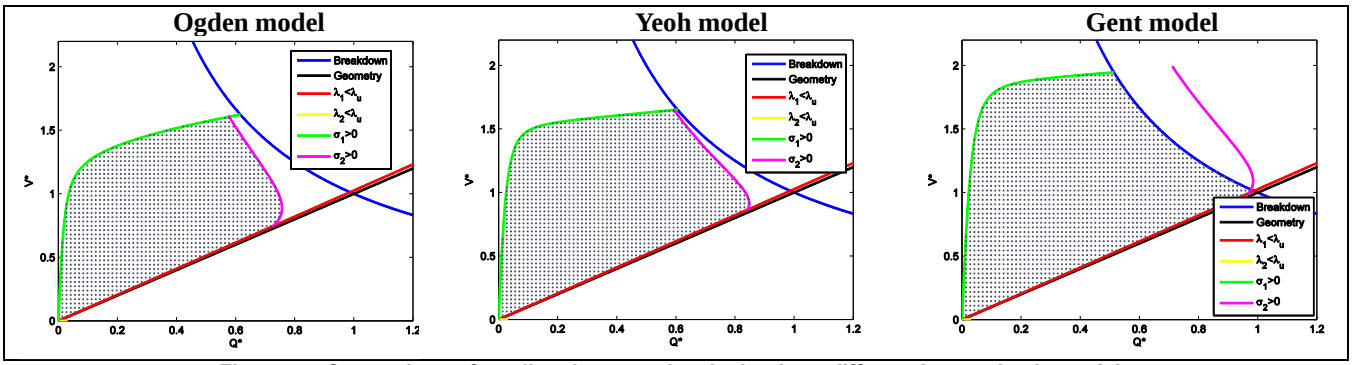

Figure 5 – Comparison of predicted energy density by three different hyper-elastic models

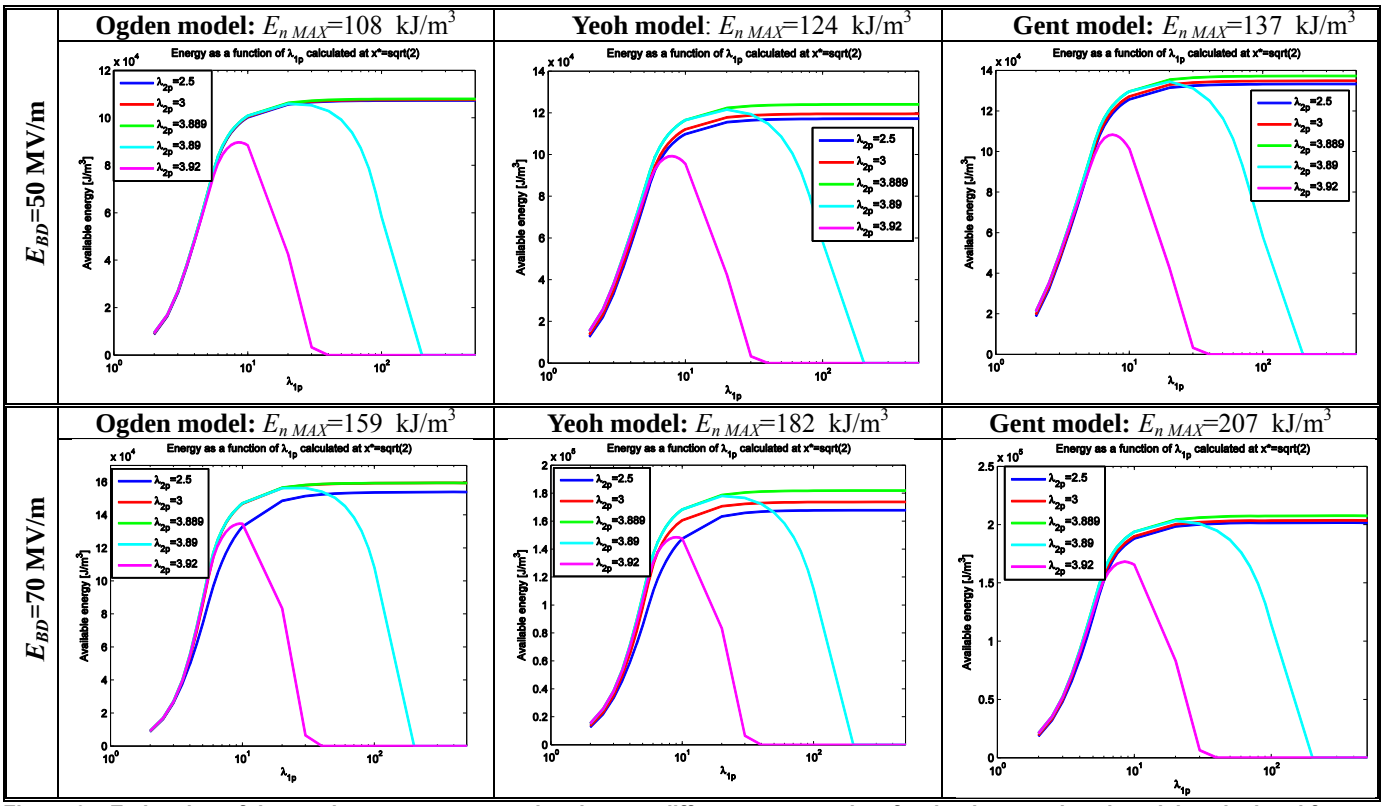

Figure 6 – Estimation of the maximum energy per unit volume at different pre-stretches for the three analyzed models calculated for two different values of dielectric strength.

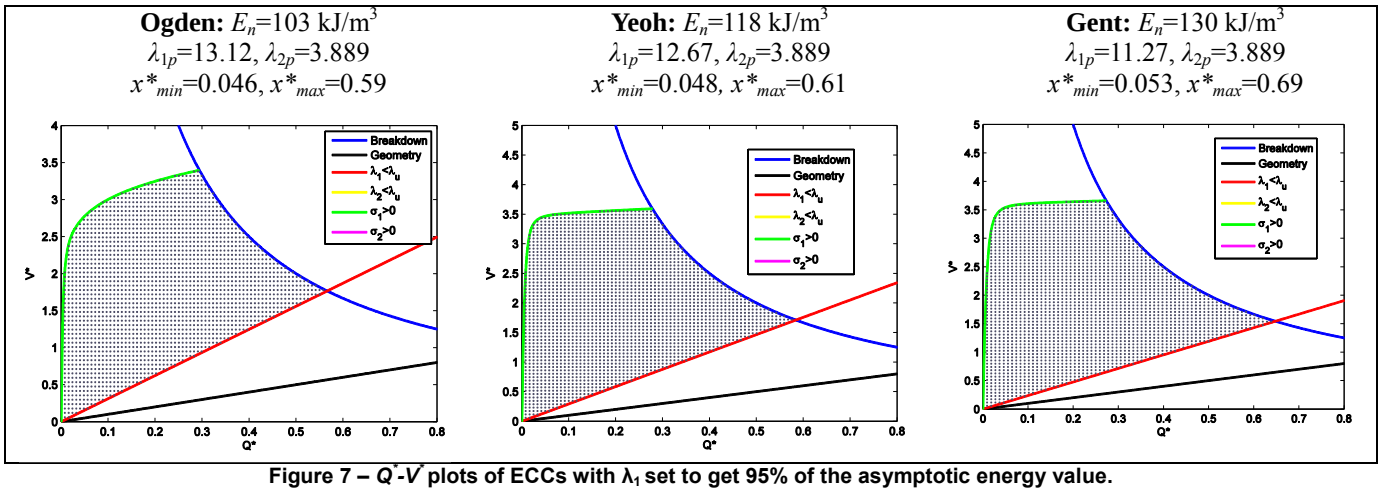

Figure 7 – Q^*-V^* plots of ECCs with λ_1 set to get 95% of the asymptotic energy value.

As shown, for an appropriate choice of λ_{2p}, the producible energy increases monotonically with λ_{1p}, reaching an asymptotic value (that is specified on the top of the graphs).

Since the maximum stretch in y direction is reached for small values of the variable x, a critical value of λ_{2p} exists so that $\lambda_2 = \lambda_u$ occurs for $x^* = 0$ (that implies $y^* = 2$). For $\lambda_u = 5.5$, it is easy to verify that this critical value is $\lambda_{2p}^c = \sqrt{2}/2\,\lambda_u \cong 3.889$.

Moreover, we can observe that:

- for $\lambda_{2p} \le \lambda_{2p}^c$, the condition $\lambda_2 < \lambda_u$ is always satisfied and the producible energy increases with λ_{1p};
- for $\lambda_{2p} \ge \lambda_{2p}^c$ the energy falls to 0 for high values of λ_{1p}. This is because the smallest reachable values of the variable x, for which λ_2 reaches the rupture value, becomes larger than the highest value of x permitted by the rupture condition on λ_1. Thus, for high values of both pre-stretches, there are no possible operative configurations for the LS-DEG;
- the dependence of the converted energy on the pre-stretch λ_{2p} (when lower than λ_{2p}^c) is weak (especially for the Ogden model); anyway, for all hyper-elastic models, the optimal condition is met when $\lambda_{2p} = \lambda_{2p}^c$;
- the three hyper-elastic models give significantly different predictions in term of maximum producible energy per unit volume;
- as expected, the producible energy increases as the dielectric strength of the DE material raises.

For the three hyper-elastic models, the optimality in terms of energy density is reached asymptotically. Figure 7 shows the ECCs (in the Q^*-V^* plane) that result from a choice of λ_{1p} that guarantees the 95% of the asymptotic value of the energy density (assuming $\lambda_{2p} = \lambda_{2p}^c$). For such ECCs, the geometric displacement range is an interval $[x^*_{min}; x^*_{max}]$. The maximum value of the LS-DEG length, x^*_{max}, is given by the rupture limit on λ_1, thus

$$x^*_{\max} = x_p^* \lambda_u / \lambda_{1p} = \sqrt{2}\,\lambda_u / \lambda_{1p}\,. \tag{29}$$

The minimum value x^*_{min} depends on the LoT limit that is close to the end of the unloading phase and that is represented by the tangent to the curve $\{\sigma_1 = 0\}$ from the origin of the axes. Specifically,

$$x^*_{min} = x_p^* \lambda_{1,min} / \lambda_{1p} = \sqrt{2}\,\lambda_{1,min} / \lambda_{1p}\,, \tag{30}$$

where $\lambda_{1,\min}$ is obtained by zeroing equation (10).

The analysis described above does not consider the presence of specific design constraints such as mechanical end-stops of realistic mechanisms, and thickness limitations of commercial DE membranes. Inclusion of constraints of this kind could yield different results as it is shown below.

A mechanical end introduces a limitation on the minimum value x^*_{min}. For E_{BD} = 50 MV/m and x^*_{min} = 0.26, Figure 8 is obtained which provides the following insights:

- the best choice for λ_{2p} is the value that brings to rupture ($\lambda_2 = \lambda_u$) when $x^* = x^*_{min}$. In this case, λ_{2p} = 3.923 is the optimum value;
- a value of λ_{1p} exists that maximizes the producible energy per unit volume.

The optimal ECCs that result from the inclusion of the constraint x^*_{min} = 0.26 are shown in Figure 9 for the three considered hyper-elastic models.

The use of commercial materials may introduce a limitation in the thickness featured by the DE membrane in its undeformed configuration. For this case, it is useful to introduce the energy per unit surface $En^S = En/\ell^2 = En\,x_0^* y_0^* t_0 / 2B$, with

$$x_0^* \ell = x_p / \lambda_{1p}\,, \quad y_0^* \ell = y_p / \lambda_{2p}\,. \tag{31}$$

Figure 10 reports the results for En^S as function of the pre-stretches for the case E_{BD} = 50 MV/m and t_0 = 1.5 mm. As shown, in case of thickness constraint, optimal values exist for both pre-stretches. Specifically, excessive values of λ_{1p} and λ_{2p} bring to very small dimensions of the DEG sample and, thus, to a significant reduction in the amount of energy that can be converted.

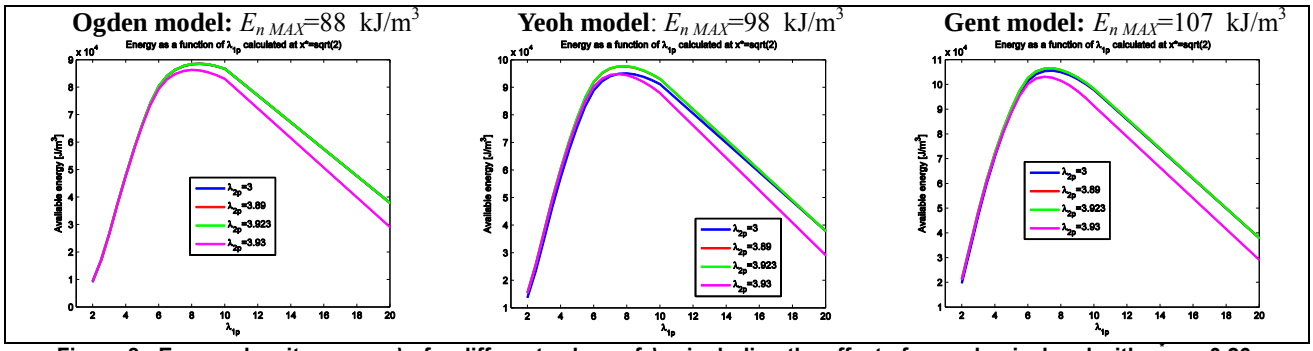

Figure 8 - Energy density versus λ_{1p} for different values of λ_{2p}, including the effect of a mechanical end with x^*_{min} = 0.26.

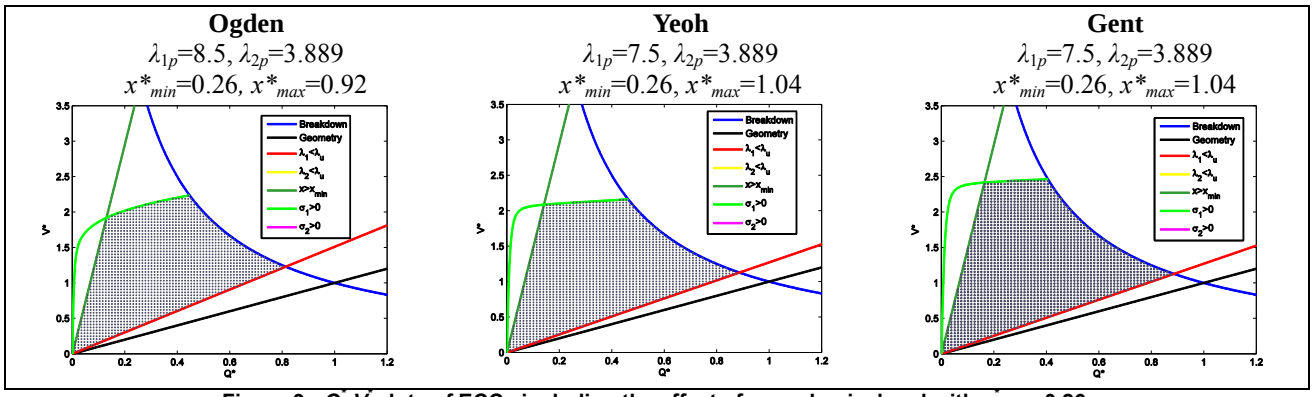

Figure 9 - Q^*-V^* plots of ECCs including the effect of a mechanical end with x^*_{min} = 0.26.

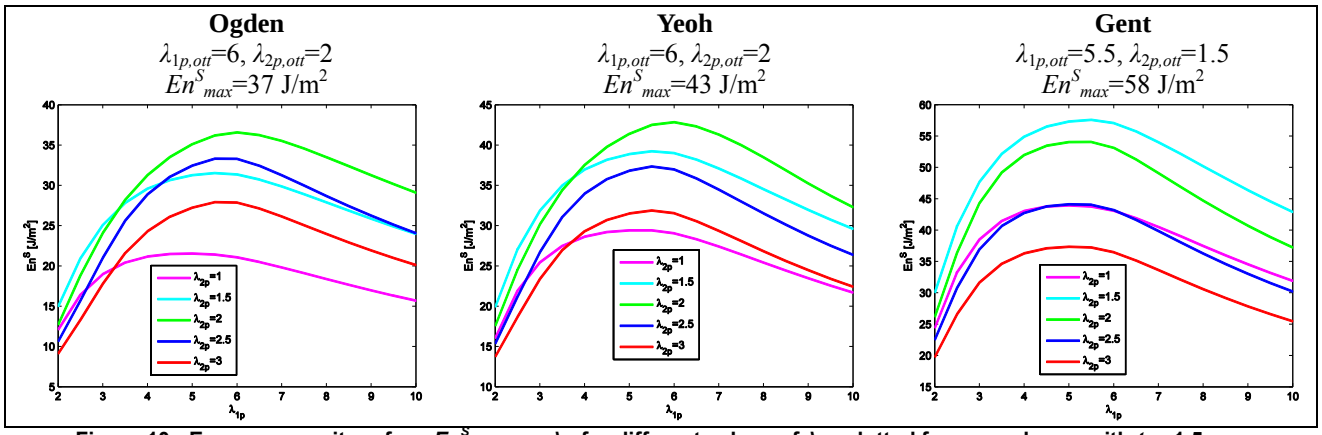

Figure 10 - Energy per unit surface En^S versus λ_{1p} for different values of λ_{2p}, plotted for a membrane with t_0 = 1.5mm.

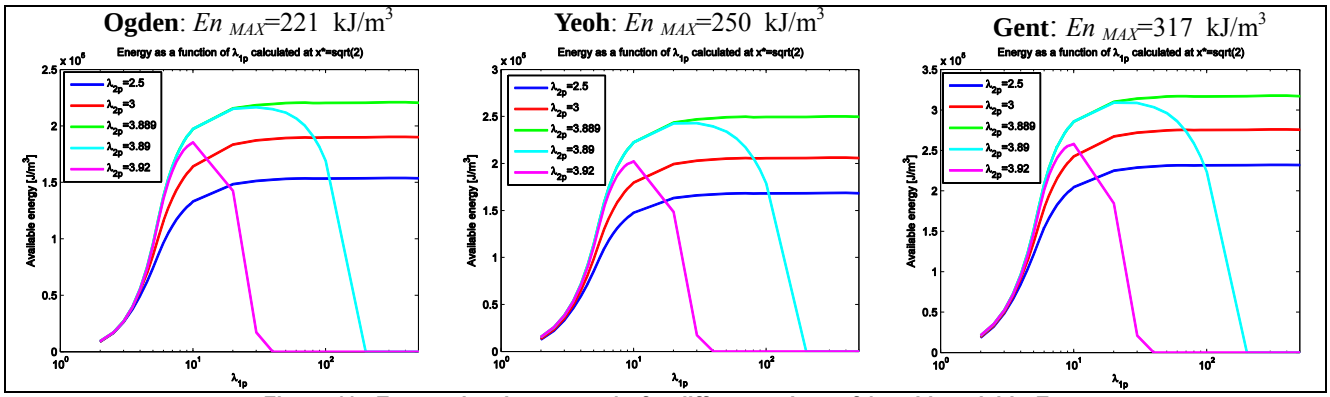

Figure 11 - Energy density versus λ_{1p} for different values of λ_{2p} with variable E_{BD}

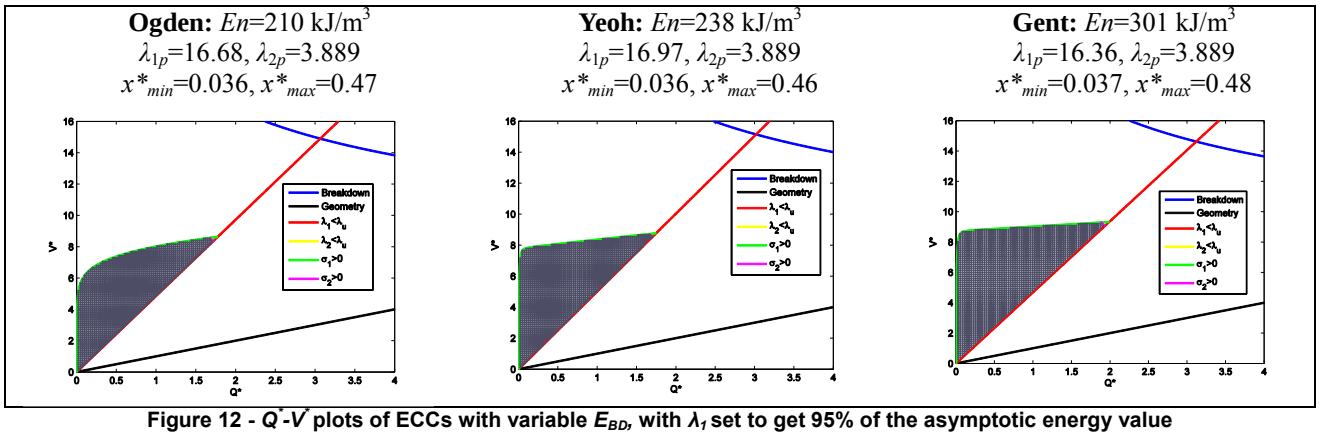

Figure 12 - Q^*-V^* plots of ECCs with variable E_{BD}, with λ_1 set to get 95% of the asymptotic energy value

Variable Electric Breakdown Condition

In the previous sub-section, the hypothesis of constant dielectric strength for the considered DE material has been used. However, the dielectric strength may depend on stretch [8]. For instance, in case of an equi-biaxial state of deformation, it can be assumed

$$E_{BD}(\lambda) = \bar{E}_{BD}\lambda^{R}, \tag{32}$$

where $\bar{E}_{BD}$ and R are constitutive constants which are specific for the considered DE material. For a different state of deformation, equation (32) can be modified as follows (see also [18])

$$E_{BD}(\lambda_1, \lambda_2) = \bar{E}_{BD}(\lambda_1\lambda_2)^{R/2}. \tag{33}$$

Accordingly, the breakdown condition (in dimensionless coordinates) is

$$Q^{*(1-R/2)}V^{*(1+R/2)} = \left(\frac{2\lambda_{1p}\lambda_{2p}}{x_p^* y_p^*}\right)^{R}, \tag{34}$$

where all the dimensionless variables are defined in equations (19)-(21).

Assuming $\bar{E}_{BD}$ = 30.6 MV/m and R = 1.13 (values suggested for the VHB-4905 by Kofod et al. in [18]) we can calculate the corresponding limit curves and maximum energy density. Results are presented in Figure 11 in terms of energy density vs. pre-stretches. Figure 12 reports the corresponding ECCs that exploit 95% of the asymptotic value of the energy density.

Differently from the case of constant E_{BD}, the plots show that the resulting ECCs are not bounded by the breakdown (BD) curve, but only by the rupture (RC) and loss-of-tension (LoT) conditions. In this particular case, the value of the dielectric strength does not represent a limitation to the maximum amount of energy that the LS-DEG can convert; thus, these values of the energy density can be considered as "upper limits" to the amount of energy that this type of device can convert.

CONCLUSIONS

Lozenge-shaped dielectric elastomer generators (LS-DEGs) have been modeled and analyzed. The maximum energy per unit volume that LS-DEGs can convert has been calculated via a failure mode analysis and for different electro-mechanical behaviors of the considered dielectric elastomer material.

The mechanical response of the material has been described using three different hyper-elastic models (Ogden, Yeoh, Gent), the parameters of which have been determined by a series of experimental tests. For each of these models, the maximum energy density that can be obtained by LS-DEGs has been estimated. Although the results of the fitting procedures are alike, the different models yield appreciable differences in term of energy conversion estimates

With a mass density of 1000 kg/m^3 for the considered dielectric elastomer material, the maximum amount of energy per unit volume that can be converted by LS-DEGs results in 0.3 J/g. This value is obtained in the hypothesis of variable dielectric strength and using a hyper-elastic model in the Gent's form.

As compared to other dielectric elastomer generator configurations based on the same material, the reported value for LS-DEGs is six times smaller than the theoretical energy density achievable by devices working in equi-biaxial deformation regimes. The limiting factor for the maximal energy density of LS-DEGs is the loss-of-tension condition, which severely affects the feasible working space of the generator (in fact, in LS-DEGs, an increase of the stretch in one direction produces a decreasing stretch in the perpendicular direction). Nonetheless, LS-DEGs are very interesting for practical applications thanks to their simplicity and easy adaptation in existing energy conversion devices featuring one degree of freedom and reciprocating motion.

Future developments of the present study may include experimental investigations on the failure conditions of available dielectric elastomer materials, as well as the implementation and field validation of LS-DEG prototypes.

ACKNOWLEDGMENTS

This work is developed in the context of the EU-FP7 project PolyWEC (www.polywec.org, prj.ref. 309139), FET-Energy.

REFERENCES

[1] Pelrine, R., Kornbluh, R., Eckerle, J., Jeuck, P., Oh, S., Pei, Q., Stanford, S., 2001, "Dielectric elastomers: Generator mode fundamentals and applications", In Proc. SPIE (Vol. 4329, pp. 148-156).

[2] Chiba, S., Waki, M., Kornbluh, R., Pelrine, R., 2008, "Innovative power generators for energy harvesting using electroactive polymer artificial muscles", 2208, Proc. SPIE 6927, Electroactive Polymer Actuators and Devices (EAPAD), 692715.

[3] Jean, P., Wattez, A., Ardoise, G., Melis, C., Van Kessel, R., Fourmon, A., Barrabino, E., Heemskerk, J.; Queau J.P., 2012, "Standing wave tube electro active polymer wave energy converter", 2012, Proc. SPIE 8340, Electroactive Polymer Actuators and Devices (EAPAD), 83400C.

[4] Vertechy, R., Fontana M., Rosati Papini, G. P., Bergamasco, M. "Oscillating-water-column wave-energy-converter based on dielectric elastomer generator" Proc. SPIE 8687, Electroactive Polymer Actuators and Devices (EAPAD), 86870I (April 9, 2013).

[5] Rosati, G.P., Vertechy, R., Fontana, M., "Dynamic Model Of Dielectric Elastomer Diaphragm Generators For Oscillating Water Column Wave Energy Converters," Proceedings of the ASME conference on smart materials, adaptive structures and intelligent systems, SMASIS2013-3255, September 16-18, 2013, Snowbird, Utah.

[6] Koh, S.J.A., Zhao, X., Suo, Z., 2009, "Maximal energy that can be converted by a dielectric elastomer generator", 2009, Applied Physics Letters 94, 262902.

[7] Jean-Mistral, C., Basrour, S, Chaillout, J-J, 2010 "Modelling of dielectric polymers for energy scavenging applications," Smart Mater. Struct. 19, 105006.

[8] Koh, S., Keplinger, C., Li, T., Bauer, S., Suo, Z., 2011, "Dielectric Elastomer Generators: how much Energy can be converted?", IEEE Transactions on Mechatronics, 16(1): 33-41.

[9] Zhu, Y., Wang, H., Zhao, D., Zhao J., 2011, "Energy conversion analysis and performance research on a cone-type dielectric electroactive polymer generator", Smart Material and Structures 20, 115022.

[10] Wang, H., Zhu, Y., Wang, L., Zhao, J., 2012, "Experimental investigation on energy conversion for dielectric Electroactive polymer generator", Journal of Intelligent Material Systems and Structures, 23(8) 885-895.

[11] McKay, T., O'Brien, B., Calius, E., Anderson, I., 2010, "Self-priming dielectric elastomer generators, Smart Mater". Struct. 19 055025.

[12] Li, T., Qu, S., Yang, W., 2012, "Energy harvesting of Dielectric Elastomer Generators concerning Inhomogeneous Fields and Viscoelastic Deformation", J. Appl. Phys. 112, 034119.

[13] Vertechy, R., Berselli, G., Parenti-Castelli, V., Vassura, G., 2010, "Optimal Design of Lozenge-Shaped Dielectric Elastomer Linear Actuator: Mathematical Procedure and Experimental Validation", Journal of Intelligent Material Systems, 21: 503-515.

[14] Morman, K.N., 2005, "Why it is necessary to use data from more than one strain field in determining the Helmoltz free-energy (strain-energy) density function", ANSOL Corporation.

[15] Holzapfel, G., 2001, "Nonlinear Solid Mechanics: a Continuum Approach for Engineering", Wiley & Sons, New York.

[16] Benjeddou, A., Jankovich, E., Hadhri, T., 1993, "Determination of the Parameters of Ogden's Law Using Biaxial Data and Levenberg-Marquardt- Fletcher Algorithm", Journal of Elastomers and Plastics, Vol. 25.

[17] Steinmann, P., Hossain, M., Possart, G., 2012, "Hyperelastic models for rubber-like materials: consistent tangent operators and suitability for Treolar's data", Archive of Applied Mechanics, Volume 82, Issue 9, pp 1183-1217.

[18] Kofod, G., Sommer-Larsen, P., Kornbluh, R., Pelrine, R., 2003, "Actuation Response of Polyacrilate Dielectric Elastomers", Journal of Intelligent Meterial Systems, 14: 787-793.